Assessing the impact of granular anaerobic membrane bioreactor intensification on treatment performance, membrane fouling and economic balance

Lucie Sanchez, Sergi Vinardell, Jules Charreton, Marc Heran, Geoffroy Lesage

Assessing the impact of granular anaerobic membrane bioreactor intensification on treatment performance, membrane fouling and economic balance

Lucie Sanchez[a], Sergi Vinardell[b,c], Jules Charreton[a], Marc Heran[a], Geoffroy Lesage[a,*]

[a] Institut Européen des Membranes (IEM), Université de Montpellier, CNRS, ENSCM, Montpellier, France

[b] Chemical Engineering Department, Escola d'Enginyeria de Barcelona Est (EEBE), Universitat Politècnica de Catalunya (UPC)-BarcelonaTECH, C/ Eduard Maristany 10-14, Campus Diagonal-Besòs, Barcelona, Spain.

[c] Barcelona Research Center for Multiscale Science and Engineering, Campus Diagonal-Besòs, Barcelona, Spain.

*Corresponding author (e-mail: geoffroy.lesage@umontpellier.fr)

ABSTRACT

Anaerobic membrane bioreactors (AnMBRs) have attracted much attention for mainstream domestic wastewater treatment. However, membrane fouling, operating costs, energy consumption and low filtration flux are important challenges slowing the scale-up of the technology. In this study and for the first time, granular sludge, submerged membrane, no gas sparging and low permeate flux were chosen to mitigate membrane fouling and to improve the energy and economic balance of an AnMBR. A granule-based AnMBR (G-AnMBR) was operated under four organic loading rates (between 0.5 and 1.6 $kgCOD.m^{-3}.d^{-1}$) with hydraulic retention times ranged from 13.9 to 4.9 hours, and instantaneous permeate flux levels ($Jp_{20,inst}$) ranged from 2.8 to 6.0 LMH to evaluate OLR impact on anaerobic digestion performance, membrane fouling extent and economic balance. Results show that COD removal rates above

83% were achieved during the four experimental periods. Membrane fouling was directly correlated to the flux and OLR and increased from 0.03 to 2.86 kPa.d^{-1} as the $Jp_{20,inst}$ increased from 2.8 to 6.0 LMH and the OLR increased from 0.5 to 1.6 kgCOD.m^{-3}.d^{-1}, respectively. In all the periods, macromolecules and colloidal proteins were the major foulants deposited on the membrane. Most of the fouling was reversible and was easily removed by physical cleaning (>97.7%). A preliminary economic assessment revealed that the permeate flux and OLR are key economic drivers for the G-AnMBR economic balance and allowed to define the satisfactory compromise between membrane purchase and chemical consumption for the long-term control of membrane fouling.

KEYWORDS

filtration flux; membrane fouling; techno-economic evaluation; granular sludge; anaerobic digestion

1. Introduction

Anaerobic membrane bioreactors (AnMBRs) have gained interest over conventional aerobic biotechnologies by combining the advantages of anaerobic processes with membrane technology. Anaerobic digestion reduces energy demand, produces fewer bio-solids, reduces sludge disposal costs and generates bioenergy through the complete conversion of organic materials into methane (Vinardell et al., 2020). Micro- or ultrafiltration membranes offer strong retention of particles and microorganisms, leading to higher biomass concentration and longer sludge retention time (SRT), which is beneficial for slow-growth anaerobic microorganisms and the quality of the permeate. Therefore, the AnMBR is a cost-effective alternative that allows conversion of wastewater organic material into renewable methane energy while achieving a high-quality effluent, free of suspended solids and pathogens, which could be easily reused for various applications (Aslam et al., 2022; Vinardell et al., 2020).

Nonetheless, the AnMBR still faces some issues that have hindered its large-scale development for domestic wastewater treatment. The main operational and technical challenges in its application to domestic wastewater have been linked to low psychrophilic temperatures, low-strength wastewater, dissolved methane and membrane fouling, among others (Aslam et al., 2022; Lei et al., 2018; Vinardell et al., 2020). The large amount of dilute domestic wastewater results in lower methane conversion rates ($L\text{-}CH_4.m^{-3}$) and higher quantities of methane lost within the effluent (Maaz et al., 2019). The loss of methane in the liquid phase diminishes the potential for energy recovery and produces direct greenhouse gas emissions (Smith et al., 2012). Membrane fouling has a high impact on the capital and operational costs of AnMBR due to its effect on permeate flux, membrane lifespan and energy demand (Maaz et al., 2019; Smith et al., 2012). Accordingly, all these factors decrease energy recovery efficiency and increase energy demand (e.g., membrane fouling mitigation, dissolved methane recovery, etc.), which reduce the economic and energy advantages of AnMBRs.

In recent years, several studies have applied lab- and pilot-scale AnMBRs to low-strength wastewater treatment at psychrophilic temperatures. As described in Table 1, various configurations and fouling control strategies have been tested to achieve high efficiencies of organic matter removal and methane conversion while mitigating membrane fouling. The chemical oxygen demand (COD) removal efficiencies obtained through AnMBR processes have typically ranged between 85% and 95% at both lab- and pilot-scales under sub-optimal conditions (i.e., ambient temperature and low-strength wastewater) (Table 1), suggesting that efficient methane yield and conversion rates can be reached (Chen et al., 2017b; Nie et al., 2017; Shin et al., 2021). Then, many investigations have focused on AnMBR configuration and membrane fouling (Table 1). The different system configurations have mainly differed in terms of (i) integration of the membrane (i.e., submerged, external submerged, side-stream), (ii) type of anaerobic bioreactor (i.e., continuous stirred tank reactor [CSTR], upflow anaerobic sludge

blanket [UASB], etc.), (iii) membrane module type (i.e., flat sheet, hollow fiber, etc.), (iv) fouling control strategies and (v) operating conditions. Innovative strategies have been implemented to better control membrane fouling (Aslam et al., 2017), including rotating membrane (Ruigómez et al., 2016a, 2016b), dynamic membrane (Hu et al., 2018; Quek et al., 2017; Yang et al., 2020), granular activated carbon media (Evans et al., 2019), sponge media (Chen et al., 2017b) and granular biomass (Chen et al., 2017a; Gouveia et al., 2015). However, gas sparging remains the most frequently used approach for long-term mitigation of membrane fouling despite its energy consumption, which amounts to up to 70% of the total AnMBR energy input (Batstone and Virdis, 2014; Smith et al., 2014).

Among the innovative strategies that have been tested, the use of granular biomass is an attractive cost-effective solution, as it reduces energy consumption for the control of membrane fouling (Martin-Garcia et al., 2013) and does not involve additional material costs or technical complexity. Granulation is a process resulting in dense granule-shaped biomass which improves biological activity and strength (van Lier et al., 2008). Unlike the suspended sludge configuration, a granule-based AnMBR (G-AnMBR) helps to lower the concentration of suspended solids in contact with the membrane, improving the control of membrane fouling and decreasing cake-layer formation (Vinardell et al., 2022). However, the G-AnMBR configuration does not fully overcome membrane fouling, as complete membrane retention leads to the accumulation of colloidal and fine particulate matter, either introduced from the influent or released from the granular sludge bed due to too strong hydrodynamic conditions (Anjum et al., 2021; Vinardell et al., 2022). To mitigate membrane fouling, gas sparging is also used in this granule-based configuration. Kong et al. (2021b) reached the maximal TMP (235 mbar) in 8 days at a filtration flux of 17.8 $L.m^{-2}.h^{-1}$ (LMH) and at a specific gas demand (SGD) of 0.75 $m^3.m^{-2}.h^{-1}$. Wang et al. (2018) applied a SGD of 0.2 $m^3.m^{-2}.h^{-1}$ and achieved the maximal TMP (550 mbar) in less than one day when the flux was increased from 5 to 10 LMH.

Gas sparging is cost-intensive and damages granule structures which increases granules fines and dissolved and colloidal organic matter (DCOM) release in the bulk (Martin-Garcia et al., 2013). For these reasons, avoiding the use of gas sparging may assist in maintaining the integrity and the particle size distribution of granules, with a substantial benefit in energy consumption (Sanchez et al., 2022). In addition, it appears that a high permeate flux cannot be maintained, which reduces the competitiveness of G-AnMBR compared to conventional processes (AeMBR). Hence, it is necessary to explore the behavior of the process following the increase of permeate flux and, more specifically, to characterize membrane fouling and its economic and energetic implications during process intensification.

This study aimed to evaluate the impact of G-AnMBR process intensification – by increasing the organic loading rate and the permeate flux – on anaerobic digestion performance, membrane fouling and process economics. The G-AnMBR system was operated without gas sparging to limit the energy consumption during domestic wastewater treatment and ambient temperature. To the best of our knowledge, the impact of process intensification on membrane fouling of a G-AnMBR in submerged mode and operated without gas sparging, has not yet been evaluated. For this reason, a G-AnMBR without gas sparging for fouling control was operated under four permeate flux conditions of 2.8, 3.6, 4.1 and 6.0 LMH and OLR of 0.5, 0.8, 1.0, 1.6 $kgCOD.m^{-3}.d^{-1}$. Anaerobic digestion performance and membrane fouling behavior were assessed. Based on the experimental results, an economic evaluation was conducted to elucidate how the intensification of the process (through OLR and permeate flux increase) might influence the operational and capital costs of a G-AnMBR operated under low filtration rates.

Table 1 – Reactor configurations, operational parameters, treatment performance and membrane fouling strategies presented in recent AnMBR studies for domestic wastewater treatment at ambient temperature.

Reactor	**Membrane setup**	**Fouling control strategy**	**Scale**	**Type of WW**	**CODin**	**T**	**HRT**	**OLR**	**$COD_{removal}$**	**Methane yield**	**Flux**	**dTMP/dt**	**Reference**
–	–	–	(liters)	–	($mg.L^{-1}$)	(°C)	(h)	($kg.m^{-3}d^{-1}$)	(%)	($L\text{-}CH_4/gCOD_{removed}$)	(LMH)	($kPa.d^{-1}$)	
UAGB	HF Sub.	Sponge cubes + intermittent cycle	(L) 3	Synthetic	330–370	20	12	–	93.7	0.156 (G)	5.3	0.5	(C. Chen et al., 2017b)
UAGB	HF Sub.	Granular sludge + Intermittent cycle	(L) 4	Synthetic	320–360	20	12	0.64–0.72 *	91.3	0.16 (G)	7	0.9	(C. Chen et al., 2017a)
UAGB	FS Sub.	Granular sludge + Intermittent cycle	(L) 6.2	Synthetic	300–350	25	13.9–4.9	0.5–1.6	83–93	70–77% [a] (G + D)	2.8–6	0.03–2.9	This study
UASB	FS sub.	Dynamic membrane	(L) 6.9	Raw	107–137	25–30	3–6	1.5–3.0	64–71	0.354 (–)	100	1.5–6.2	(Quek et al., 2017)
UAGB	HF Ext. sub.	Granular sludge + Intermittent cycle + gas sparging	(P) 72.5	Raw	221	16.3	8	<1.0 *	83	–	5–15	0.2–960 *	(Wang et al., 2018)
UAGB	HF Sub.	Granular sludge + Intermittent cycle + gas sparging	(P) 459	Raw	978	18	9.8–20.3	0.72–3.18	≈90	0.216–0.226 (G + D)	10–14	0.1–1.9	(Gouveia et al., 2015)
CSTR	FS Sub.	Intermittent cycle + gas sparging	(L) 6	Synthetic	700	25	8–48	0.35–2.1	≈95	0.277–0.328 (G + D)	1.1–6.5	–	(R. Chen et al., 2017a)
CSTR	FS Sub.	Intermittent cycle + gas sparging	(L) 6	Synthetic	700	25	8–48	0.35–2.1	>90	0.305–0.338 (G + D)	1.1–6.5	0.05–1.1 *	(R. Chen et al., 2017b)
CSTR	– Sub.	Gas sparging	(L) 6	Synthetic	492	25	24–12	3–6	97–94	89–84.7% [a] (G + D)	–	0.08–0.3	(Nie et al., 2017)
CSTR	FS Sub.	Intermittent cycle + gas sparging	(L) 40	Raw	428–477	14–26	12–48	0.23–0.9	69–89	0.28–0.35 *,[b] (G + D)	1.6–6.6	<0.06 *	(Plevri et al., 2021)
CSTR	HF Ext. sub.	Gas sparging	(P) 630	Synthetic	304–388	23	8.5	0.85–1.1 *	88–92	0.076–0.115 (G + D)	17	0.02–0.61	(Dong et al., 2016a, 2016b)

AFBR	HF Sub.	Granular activated carbon + gas sparging	(P) 990	Raw	210	13–32	3.9	1.3–1.4	86–90	0.17 (G)	7.6–7.9	–	(Evans et al., 2019)
AFBR	HF Ext. sub.	Intermittent cycle + gas sparging	(P) 4500	Raw	720–893	18–25	5.3–10	1.3–2.4	87–90	43–62 % [a] (G + D)	6.5–12.3	–	(Shin et al., 2021)
–	HF Sub.	Intermittent cycle + gas sparging	(P) 20	Raw	422	25	4–12	1.52–0.72	84–89	0.14–0.21 (G + D)	7.2–14.2	0.8–2.1	(Ji et al., 2021a)
–	HF Sub.	Gas sparging	(P) 20	Raw	422	15–25	6	0.15–0.18	77–90	0.06–0.17 (G + D)	9.5	0.1–13.0	(Ji et al., 2021b)
–	HF Sub.	Gas sparging	(P) 20	Raw	300–600	15	6–24	0.4–1.6	77–91	0.06–0.23 (G + D)	2.4–9.4	1.4–9.1	(Ji et al., 2022)
–	HF Sub.	Intermittent cycle + gas sparging	(P) 5000	Raw	403–461	25–27	6–24	0.37–1.84	90–93	0.16–0.26 (G + D)	4.4–17.8	0.08*–2.9	(Kong et al., 2021a) (Kong et al., 2021b)
–	HF Ext. sub.	Intermittent cycle + Gas sparging	(P) 40000	Raw	1235	27–30	24–60	–	92	0.21 (G + D)	15–23.5	0.04–0.22	(Robles et al., 2020)
–	HF Sub.	Intermittent cycle + Gas sparging	(P) 5000	Raw	414	25	8	1.2	90	0.222 (G + D)	10.85	0.04–0.2	(Rong et al., 2021)
–	HF Sub.	Rotating membrane	(L) 3	Raw	1462	19	33	–	91	0.154 * (G)	10	3.8*–14	(Ruigómez et al., 2016a, 2016b)
–	– Sub.	Gas sparging	(L) 6	Synthetic	491	10–25	6–48	0.25–1.0	71–98	32–77 % [a] (G)	–	0.17–0.72	(Watanabe et al., 2017)
UASB	– Sub.	Dynamic membrane	(L) 3.6	Raw	251–284	20–25	1–8	0.8–6.8	60–77	0.05–0.12 (G + D)	22.5–180	0.4–2.1	(Yang et al., 2020)

WW: wastewater; HRT: hydraulic retention time; OLR: organic loading rate; UAGB: upflow anaerobic granular bioreactor; UASB: upflow anaerobic sludge blanket; CSTR: completely stirred reactor; AFBR: anaerobic fluidized bed reactor ; FS: flat sheet; HF: hollow fiber; Sub.: membrane submerged in the bioreactor; Ext. sub.: membrane submerged in an external tank; L: lab-scale; P: pilot-scale; G: gaseous methane; D: dissolved methane.

* Values were calculated or approximated through data available in the publication.

[a] Methane conversion rate (%)

[b] Values were calculated based on the gas yield provided, considering a concentration of CH_4 of 70%.

2. Materials and methods

2.1 G-AnMBR setup

The G-AnMBR system consisted of a parallelepipedic tank (266 × 68 × 523 mm) with a working volume of 6.2 L that was operated in continuous mode for 357 days. The membrane module was immersed in the middle of the liquor (at a height of 205 mm from the bottom). The ultrafiltration membrane was a polyethersulfone (PES) flat-sheet membrane with a pore size of 0.04 µm (Microdyn Nadir®, Germany). The module was composed of six membrane sides, providing a total surface area of 0.34 m². The permeate was suctioned through a peristaltic pump (LeadFluid®, China) following an operation cycle of 8 min 15 s of filtration, 30 s of relaxation, 45 s of backwash and 30 s of relaxation. No method for the mitigation of membrane fouling was used apart from the intermittent cycle. The operation of the reactor was automatically managed by automation software developed by AC2I Automation (France). The reactor was thermoregulated at 25°C. The influent was fed at the bottom of the reactor by a peristaltic pump and diffused over the entire length by a pierced hollow tube (ø 1 mm) to minimize dead zones. Continuous recirculation from the top to the bottom of the reactor was used to provide an upflow liquid velocity (ULV) of 2.6 m/h (Boulenger and Gallouin, 2009) and no other mixing that this recirculation was operated. A schematic representation of the lab-scale reactor is shown in Fig. A1.

A complex synthetic influent was used to mimic domestic wastewater treatment, as described in previous studies (Layer et al., 2019; Sanchez et al., 2022). The feed solution was prepared every week with and stored at 4°C for one week. During the overall experiment, the average composition of the influent was approximately 290–350 $mgCOD.L^{-1}$ for total COD (tCOD), 250–290 $mgCOD.L^{-1}$ for soluble COD (sCOD), 40–60 $mgCOD.L^{-1}$ for particulate COD (pCOD) and 160–210 $mgCOD.L^{-1}$ for volatile fatty acids (VFA).

The G-AnMBR was inoculated with granular sludge from a mesophilic (35–38°C) UASB that treats wastewater from a recycled paper factory (Saica Paper Champblain-Laveyron, France) at a high organic loading rate (18 $kgCOD.m^{-3}.d^{-1}$). The granular sludge was acclimatized stepwise to the low-strength (0.5 $kgCOD.m^{-3}.d^{-1}$) and psychrophilic temperature (25°C) for 20 months before the beginning of this study. The total solids concentration in the G-AnMBR was 70–80 $gTS.L^{-1}$. No sludge was purged during the 357 days of the experiment except for sampling.

2.2 Experimental design and operating conditions

Four experimental periods were used to assess the impact of design parameters on G-AnMBR performance, membrane fouling behavior and economic assessment. The influent flow was progressively increased, with a direct impact on hydraulic retention time (HRT), organic loading rate (OLR) and permeate flux (J_{20}). The G-AnMBR was then operated according to the following conditions: instantaneous filtration fluxes ($J_{20,inst}$) of 2.8, 3.6, 4.1 and 6.0 LMH, HRT from 14 to 5 h, and OLR from 0.5 to 1.6 $kgCOD.m^{-3}.d^{-1}$ (Table 2), which are within the common range of AnMBR studies for domestic WW treatment (Vinardell et al., 2020). The end of each period was reached when a steady efficiency of COD removal was achieved and the fouling rate was constant and considered to be sufficiently long to be representative of the period. The maximal TMP recommended for the membrane supplier was 400–500 mbar.

167 Table 2 – G-AnMBR operating conditions during the different operating periods.

Parameters	Period 1	Period 2	Period 3	Period 4
Days of operation (d)	1–134	135–203	204–289	290–357
$Jp_{20,inst}$ (LMH)	2.8 ± 0.1	3.6 ± 0.1	4.1 ± 0.3	6.0 ± 1.4
$Jp_{20,net}$ (LMH)	1.3 ± 0.1	1.8 ± 0.1	2.5 ± 0.2	3.6 ± 1.2
HRT (h)	13.9 ± 0,5	9.9 ± 0.3	7.0 ± 0.7	4.9 ± 1.4
OLR ($kgCOD.m^{-3}.d^{-1}$)	0.5 ± 0.1	0.8 ± 0.2	1.0 ± 0.4	1.6 ± 0.7
Temperature (°C)	25.0 ± 0.3	25.0 ± 0.8	24.9 ± 1.2	25.3 ± 2.0
pH (–)	7.2 ± 0.6	7.0 ± 0.2	7.3 ± 0.2	7.4 ± 0.2
Redox (mV)	–488 ± 22	–488 ± 17	–494 ± 14	–478 ± 23
ULV ($m.h^{-1}$)	2.6 ± 0.03	2.6 ± 0.03	2.6 ± 0.03	2.6 ± 0.03

168

169 **2.3 Membrane fouling indicators**

170 The extent of membrane fouling was evaluated through the monitoring of transmembrane
171 pressure (TMP). A pressure gauge was installed on the permeate line, and data were recorded
172 every 15 seconds. Data processing allowed calculation of the average maximal TMP per day.

173 Filtration resistance analysis was used to understand fouling mechanisms. Fouling resistance
174 was measured using Darcy's law (Eq. 1) and the resistance-in-series model (Eq. 2).

$$R_t = \frac{TMP}{\mu_{20}.J_{20}} \quad \text{Eq. 1}$$

$$R_t = R_m + R_f = R_m + (R_{reversible} + R_{irreversible} + R_{residual}) \quad \text{Eq. 2}$$

175 where R_t is the resistance (m^{-1}), TMP is the transmembrane pressure (Pa), J_{20} is the normalized
176 flux at 20°C ($L.m^{-2}.h^{-1}$), μ_{20} is the viscosity of water at 20°C (Pa.s), R_m is the membrane
177 resistance (m^{-1}), R_f is the fouling resistance (m^{-1}) and $R_{reversible}$, $R_{irreversible}$ and $R_{residual}$ are the
178 resistances caused by reversible fouling, irreversible fouling and residual fouling, respectively
179 (m^{-1}).

All resistances were measured by filtering deionized water through the membrane. R_m was measured with a clean membrane, R_t was measured at the end of experimental periods with a fouled membrane and R_f was deduced. Subsequently, the fouled membrane was physically cleaned by water rinsing with 5 L of deionized water allowing for calculation of $R_{reversible}$. Finally, the membrane was chemically cleaned by soaking (2 h) in a 0.2% NaOCl solution, providing the resistance removed by chemical cleaning $R_{irreversible}$ and the residual resistance $R_{residual}$.

2.4 Analytical procedures

Influent, supernatant and effluent were sampled twice per week to measure the tCOD and sCOD concentration using commercial kits (Hach, Germany, LCK 500, 314, 514). The supernatant was sampled on the liquid recirculation line. The sCOD concentration was measured after pre-filtration at 0.45µm. sCDO removal was divided into 'biological removal' and 'membrane removal' (section 3.1.1). The sCOD removed between influent and supernatant was associated to 'biological removal' whereas the sCOD removal measured between supernatant and permeate was related to 'membrane removal'. It should be noticed that the 'membrane removal' takes into account the membrane barrier rejection and the potential biological removal by the biofilm developed on membrane surface. VFAs were analyzed regularly by ion-exclusion chromatography (ICS-900, Dionex, USA; column BP-OA_2000, Benson Polymeric Inc., USA) coupled with UV detector (210 nm). H_2SO_4 (0.05N) was used as eluent at 0.4 $mL.min^{-1}$. Six VFAs were quantified, namely acetic acid, propionic acid, butyric acid, iso-butyric acid, iso-valeric acid and valeric acid. All samples were passed through a 0.22 µm filter prior to HPLC-UV analysis. Mixed liquor suspended solids were measured according to standard methods (APHA et al., 1998).

A three-dimensional fluorescence excitation emission matrix (3DEEM) was used to characterize the composition of the DCOM of the foulant. After physical cleaning, the collected

foulant was mixed thoroughly and pre-filtered through a 1.2 µm filter to conserve the colloidal compounds. A fluorescence spectrophotometer (FL 6500, Perkin-Elmer, USA) was used with excitation and emission scan ranges of 200–500 nm and 280–600 nm, respectively. Data analysis was performed according the protocol of Jacquin et al. (2017). Three regions of fluorophores were distinguished, namely (a) region I + II, associated with protein-*like* molecules, (b) region IV, corresponding to soluble microbial product (SMP)-*like* molecules, and (c) region III + V, related to humic substances.

Quantification of proteins (PN) and polysaccharides (PS) was conducted following the Lowry and Dubois methods, respectively (Dubois et al., 1951; Lowry et al., 1951). Bovine serum albumin (BSA) and glucose were used as standards. All samples were pre-filtered through a 0.45 µm filter before PN and PS quantification.

The extracellular polymeric substances (EPS) of the fouling layer were quantified because they play a key role in membrane fouling. The EPS basically can be divided into three fractions depending on their structure: soluble EPS, also known as soluble microbial products (SMPs), loosely-bound EPS (LB-EPS) and tightly-bound EPS (TB-EPS). The heating extraction method described by Li and Yang (2007) was used. The concentration of each EPS fraction was quantified as the sum of PN and PS contents.

2.5 COD mass balance

The COD mass balance (gCOD.d^{-1}) was determined according to Eq. 3.

$$tCOD_{in} = tCOD_{out} + COD_{CH4}^{G} + COD_{CH4}^{L} + COD_{SO4} + \Delta COD_{biomass} \quad \text{Eq. 3}$$

where $tCOD_{in}$ and $tCOD_{out}$ are the tCOD concentrations experimentally measured in the influent and effluent (mg.L^{-1}), respectively; COD_{CH4}^{G} and COD_{CH4}^{L} are the equivalent COD concentrations of the produced gaseous and dissolved methane, respectively; COD_{SO4} corresponds to the COD used for the reduction of sulfate by sulfate-reducing bacteria (0.67

228 gCOD.gSO$_4^{-1}$); and $\Delta COD_{biomass}$ is the COD used for biomass synthesis (0.1 gVSS.gCOD^{-1}).
229 The dissolved methane (COD_{CH4}^{L}) was quantified experimentally following the headspace
230 method described by Sanchez et al. (2022). Total methane produced was calculated using the
231 theoretical value of 0.38 L-CH$_4$/gCOD$_{removed}$ at 25°C, allowing for the gaseous methane
232 (COD_{CH4}^{G}) calculation.

233 **2.6 Preliminary economic evaluation**

234 The economic assessment was conducted for four scenarios, corresponding to the four operating
235 periods. The design parameters, process performance and membrane fouling rates of the four
236 experimental periods were used for the calculations. The economic analysis was performed
237 considering a wastewater flow rate of 20,000 m^3.d^{-1} (i.e. 100,000 population equivalent).
238 Detailed information of the design criteria for each scenario can be found in Table A1 of the
239 supplementary data.

240 The capital and operating costs influenced by permeate flux, membrane fouling rate and process
241 performance were included in the economic evaluation. For this reason, the costs not influenced
242 by the evaluated parameters have not been included in the economic evaluation because they
243 are expected to be similar for the four scenarios. Capital expenditures (CAPEX) comprised the
244 purchase of the membranes, the bioreactor construction and the combined heat and power
245 (CHP) unit for biogas valorization. Operational expenditures (OPEX) comprised the chemical
246 reagents needed for membrane chemical cleaning, energy consumption for CHP unit and the
247 equipment replacement cost (i.e., membrane and CHP unit). Revenues corresponded to the
248 energy recovered from the biogas. All design and cost parameters used to calculate costs and
249 revenues are provided in Table A3 of the supplementary data.

250 The chemical cleaning protocol was adapted from Brepols et al. (2008) and used a 0.05%
251 NaOCl solution (2 h) and a 2,000 mg.L^{-1} citric acid solution (2 h). A chemical cleaning was

252 considered required when the maximal applicable TMP of 400 mbar was reached. It was
253 assumed that the initial membrane permeability was recovered after each chemical cleaning.
254 Chemical cleanings have an impact on membrane lifetime because the chemicals damage the
255 membrane materials and modify their properties and performance (Chheang et al., 2022). The
256 replacement of the membrane was presumed to be conducted when a maximum cumulative
257 chlorine contact of 500,000 $mg.L^{-1}.h^{-1}$ was reached (Robles et al., 2014; Vinardell et al., 2022).

258 The present value of the net cost (PV_{NC}) was calculated for the four scenarios as the difference
259 between the PV of the gross cost (CAPEX + OPEX) and the PV of the electricity revenue
260 considering three plant lifetimes (i.e., 20, 30 and 40 years) and a discount rate of 5%. Detailed
261 information regarding the equations used for the economic evaluation can be found in Table
262 A3 of the supplementary data.

263 # 3. Results and discussion

264 ## 3.1 Overall treatment performance

265 ### 3.1.1 Biological and membrane rejection performances

266 Table 3 summarizes the average tCOD, VFA and MLSS values for the four periods. The tCOD
267 removal efficiency ranged between 82.5% and 92.6%, with average tCOD concentrations in the
268 effluent varying from 22.5 to 52.9 $mgCOD.L^{-1}$, which was in compliance with European Union
269 discharge standards (Directive 91/271/EEC). The MLSS in the permeate were below 5 $mg.L^{-1}$
270 in every experimental period, which was considerably below the 35 $mgSS.L^{-1}$ regulation
271 discharge (Directive 91/271/EEC). The concentration of MLSS in the supernatant slightly
272 increased with the decrease of HRT (Pearson's correlation coefficient $r = –0.852$). This result
273 was expected because (i) ultrafiltration membranes retain particulate matter, which can
274 accumulate over time and (ii) lower HRT induces higher OLR, increasing levels of particulate
275 and colloidal materials and thus promoting biomass growth (R. Chen et al., 2017b; Huang et

al., 2011). Solid concentration build-up near the membrane has been previously correlated with TMP increase (Gouveia et al., 2015).

Table 3 – Influent and effluent compositions and removal efficiencies (mean values ± SD; $n \geq 10$).

Parameters	Units	Period 1	Period 2	Period 3	Period 4
OLR	$kgCOD.m^{-3}.d^{-1}$	0.5 ± 0.1	0.8 ± 0.2	1.0 ± 0.4	1.6 ± 0.7
$tCOD_{in}$	mgCOD/L	311.4 ± 54.7	346.4 ± 63.8	303.0 ± 91.0	298.8 ± 74.5
$tCOD_{eff} = sCOD_{eff}$	mgCOD/L	22.5 ± 7.7	24.8 ± 7.4	32.7 ± 17.6	52.9 ± 28.4
$tCOD_{removal}$	%	92.4 ± 3.1	92.6 ± 2.2	89.1 ± 4.7	82.5 ± 7.7
VFA_{inf}	mgCOD/L	209.2 ± 43.2	159.2 ± 38.0	170.7 ± 10.0	190.3 ± 11.1
VFA_{eff}	mgCOD/L	0.0 ± 0.0	3.6 ± 4.6	2.3 ± 1.7	1.6 ± 2.2
$VFA_{removal}$	%	100 ± 0	97 ± 4	96 ± 5	99 ± 1
$MLSS_{supernatant}$	mg/L	88 ± 50	179 ± 108	209± 106	194 ± 99
$MLSS_{eff}$	mg/L	3.6 ± 3.9	1.3 ± 2.1	1.8 ± 0.7	3.8 ± 2.8

Fig. 1a presents the distribution of sCOD removal during the different periods. Under all conditions, 10 ± 1.5% of the sCOD influent was removed by the physical membrane barrier and/or by the biomass attached to the membrane surface. This highlights that the effectiveness of membrane separation was not affected by the filtration flux. The retention of particulate matter and some DCOM by the membrane was observed to improve effluent quality further and enhance the removal rate of organic material (Gouveia et al., 2015; Sanchez et al., 2022; Smith et al., 2013). No statistical difference was observed among the tCOD removal efficiencies achieved in all experimental periods ($p > 0.05$) with the exception of Period 4.0 ($p < 0.05$). In this latter case, when the OLR increased from 1.0 to 1.6 $kgCOD.m^{-3}.d^{-1}$, biological sCOD removal dropped to 57%. The G-AnMBR performances rose progressively for 45 days until reaching an average biological sCOD removal of 80.6 ± 5.5 and a tCOD removal rate of 92.7 ± 1.5%. Thus, the anaerobic microbial community eventually adapted to harsh operational conditions, probably due to membrane retention that uncoupled HRT and SRT and thus allowed for acclimation of anaerobic bacteria and archaea (Stuckey, 2012). These results are consistent

with those obtained by Ji et al. (2021), who operated a submerged AnMBR for domestic wastewater treatment at 25°C under different operating conditions. For an OLR between 1.5 and 0.7 kgCOD.m^{-3}.d^{-1} (HRT 6–12 h), a steady high COD removal efficiency above 89% was observed. However, the biological performance substantially decreased at an OLR of 2.1 kgCOD.m^{-3}.d^{-1} (HRT 4h), although the organic material retained by the membrane compensated for the decrease in bioactivity (Ji et al., 2021a).

Fig. 1b shows the VFA concentrations measured in the influent, supernatant and effluent of the G-AnMBR. The VFA concentration is expressed as the sum of all VFAs converted into COD equivalents. Among the VFAs analyzed, acetic acid and propionic acid were the predominant compounds (10–120 mg/L); butyric acid, iso-butyric acid and iso-valeric acid were near the limit of quantification (<2 mg.L^{-1}); and valeric acid was below the level of detection (<0.5 mg.L^{-1}). VFAs are key intermediate products of anaerobic digestion and their concentrations within the mixed liquor give an indication about the process stability and the proper functioning of methane-producing archaea (van Lier et al., 2008). The lower the amount of VFA, the more efficient the anaerobic reaction chain. Low amounts of VFAs were measured, and no VFA accumulation was observed in the G-AnMBR supernatant during the experimental periods. This analysis confirms that (i) a steady state was reached and (ii) the anaerobic bacteria and archaea were consistent with all the conditions evaluated. Furthermore, Fig. 1b reveals very low VFA concentration in the permeate (1.9 ± 1.3 mgCOD.L^{-1}), revealing that these compounds were biologically degraded and additionally removed in the membrane separation step (Fig. 1b). Theoretically, VFAs could pass through the membrane due to their low molecular weight but this phenomenon has been previously observed, demonstrating the positive impact of fouling layer biological activity (Chen et al., 2017a; Martinez-Sosa et al., 2011). Previous studies have hypothesized that the biomass attached to membrane surface is considerably active, even more active than suspended biomass, because of lower mass-transfer limitations (Smith et al., 2013).

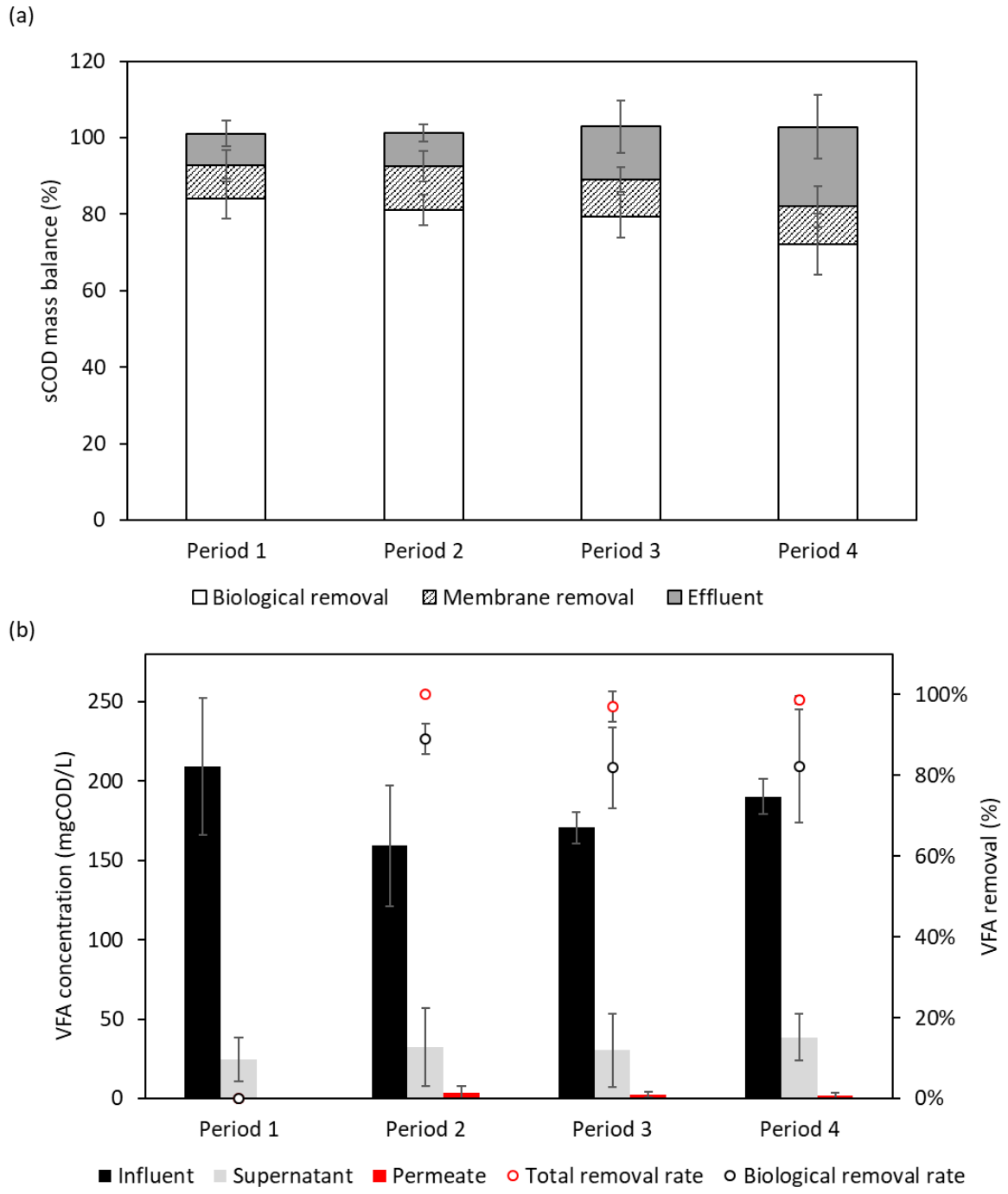

Fig. 1 – (a) Distribution of sCOD biological removal, membrane removal and effluent content; (b) VFA concentration and removal efficiency under all operating conditions (HRT 14, 10, 7, 5 h; OLR 0.5, 0.8, 1.0, 1.6 $kgCOD.m^{-3}.d^{-1}$ for periods 1, 2, 3 and 4, respectively).

3.1.2 COD mass balance

COD mass balance distribution for the four operational conditions is provided in Table 4. The COD contained in the effluent and the methane production were the two major factors affected by the changes in OLR. As expected, the quantity of COD_{in} converted into methane increased

considerably, from 2.7 to 7.4 gCOD.d^{-1} (2.7-fold), and the influent flux increased from 3.55 to 10.70 gCOD.d^{-1} (3-fold). However, the fraction of the tCOD converted into methane decreased from 77% to 70% as the OLR increased from 0.5 to 1.6 kg.m^{-3}.d^{-1}, respectively. At the same time, the proportion of COD_{in} retrieved as dissolved methane (lost methane) decreased from 27% to 10% when the OLR increased (Table 4). These results indicate that a trade-off must be found in the applied operating conditions to enable both a high rate of conversion of organic matter to methane and a lower concentration of dissolved methane.

Dissolved methane measured during the periods was lower as OLR increased (r = –0.95). Specifically, dissolved methane concentration was 21.2 ± 1.3 mg.L^{-1} for Period 1, 20.5 ± 2.4 mg.L^{-1} for Period 2, 14.7 ± 2.1 mg.L^{-1} for Period 3 and 9.3 ± 3.0 mg.L^{-1} for Period 4. Similarly to the present study, Yeo et al. (2015) observed that the fraction of dissolved methane (relative to the total methane produced) decreased from 35 to 14% as the OLR increased from 0.4 to 1.1 kgCOD.m^{-3}.d^{-1}. The increase in gas production at higher OLR levels led to an increase in local turbulence and mass transfer, allowing more methane to escape the liquid phase and diminishing the level of supersaturation (Yeo et al., 2015).

Table 4 – COD mass balance during each experimental period.

Period	1		2		3		4	
	gCOD.d^{-1}	%	gCOD.d^{-1}	%	gCOD.d^{-1}	%	gCOD.d^{-1}	%
Influent COD	**3.55**	**100**	**5.50**	**100**	**7.10**	**100**	**10.70**	**100**
Effluent COD	0.27	8	0.41	7	0.83	12	1.74	16
Sludge growth	0.47	13	0.72	13	0.89	13	1.27	12
Sulfate reduction	0.10	3	0.16	3	0.20	3	0.28	3
Dissolved CH_4	0.95	27	1.34	24	1.37	19	1.04	10
Gaseous CH_4	1.77	50	2.86	52	3.82	54	6.37	60
Total CH_4	2.72	77	4.20	76	5.19	73	7.41	70

3.2 Membrane fouling behavior

3.3.1 Membrane filtration performance

Fig. 2 shows the extent of membrane fouling through the TMP evolution along the operational periods. Table 5 provides the membrane fouling rates obtained from the TMP profiles. Substantial differences in TMP profiles were observed between each period. During Period 1 ($Jp_{20,net}$ = 2.8 LMH), TMP slowly increased to 46 mbar with a progressive rise of 0.03 kPa.d^{-1} (Table 5). The very low membrane fouling rate suggests that the membrane was operating at sub-critical filtration flux, as no severe fouling was observed. When the instantaneous filtration flux was increased to 3.6 LMH (Period 2), the TMP reached 305 mbar (ΔTMP = 236 mbar) after 65 days of filtration. The TMP profile was characterized by a slow upward trend (0.16 kPa.d^{-1}), followed by a much faster fouling rate (0.87 kPa.d^{-1}), resulting in an average fouling rate estimated at approximately 0.40 kPa.d^{-1} (Table 5). In Period 3 ($Jp_{20,inst}$ = 4.1 LMH), TMP rapidly and steadily increased, with an average daily rise of 0.65 kPa.d^{-1}, until a maximal TMP of 430 mbar was reached. During Period 4, the initial filtration flux targeted ($Jp_{20,inst}$ = 7.5 LMH) led to very strong and fast membrane fouling; the average instantaneous flux in this period was of 6.0 ± 1.4 LMH. The TMP increased from 40 mbar to 530 mbar within 9 days (day 290 to 299), and constant instantaneous filtration flux was unable to be sustained, thus decreasing slowly to 5.7 LMH. On day 303, the membrane was removed from the reactor for physical and chemical cleaning. The filtration for Period 4 was restarted, and the same sharp upward trend in TMP was observed after the membrane cleaning. The membrane fouling rate was approximately 2.86 kPa.d^{-1}. On day 316, the maximal TMP was reached; then, the instantaneous permeate flux dropped progressively to 4.1 LMH until the end of the experiment. The concept of critical flux states that under fixed operating conditions (e.g., MLSS, hydrodynamics conditions, membrane properties) there is a threshold flux above which a sustainable flux cannot be further maintained (Bacchin et al., 2006). Fig. 2 clearly shows that

apart from Period 1 ($Jp_{20,inst}$ = 2.8 LMH), the critical flux was exceeded because apparent fouling was observed during the experimental periods. Conversely, a critical instantaneous flux of 5 LMH was obtained in a mesophilic (30°C) AnMBR at a TSS concentration of 50 $g.L^{-1}$ when gas sparging (U_g = 35 m/h) was applied (Jeison and van Lier, 2006). The lower critical flux obtained in this study can be attributed to the very high concentration of solids and the poor shear rate due to the absence of gas sparging.

These results confirm that the TMP substantially increased with the permeate flux, which confirms the high impact of permeate flux on membrane fouling. The increase in filtration flux led to higher convective forces in such a way that foulants were pushed toward the membrane surface more harshly and quickly; thus, the lift and diffusion forces had less effect in carrying foulants away (Chen et al., 2017a).

Table 5 – Fouling rates at different filtration conditions.

Period	Filtration conditions	Fouling rates	
	$Jp_{20,inst}$ (LMH)	$dTMP/dt$ ($kPa.d^{-1}$)	dR/dt ($m^{-1}.d^{-1}$)
1	2.8 ± 0.1	0.03	0.9×10^{11}
2	3.6 ± 0.1	0.40	9.3×10^{11}
3	4.1 ± 0.3	0.65	10.3×10^{11}
4	6.0 ± 1.4	2.86	34.0×10^{11}

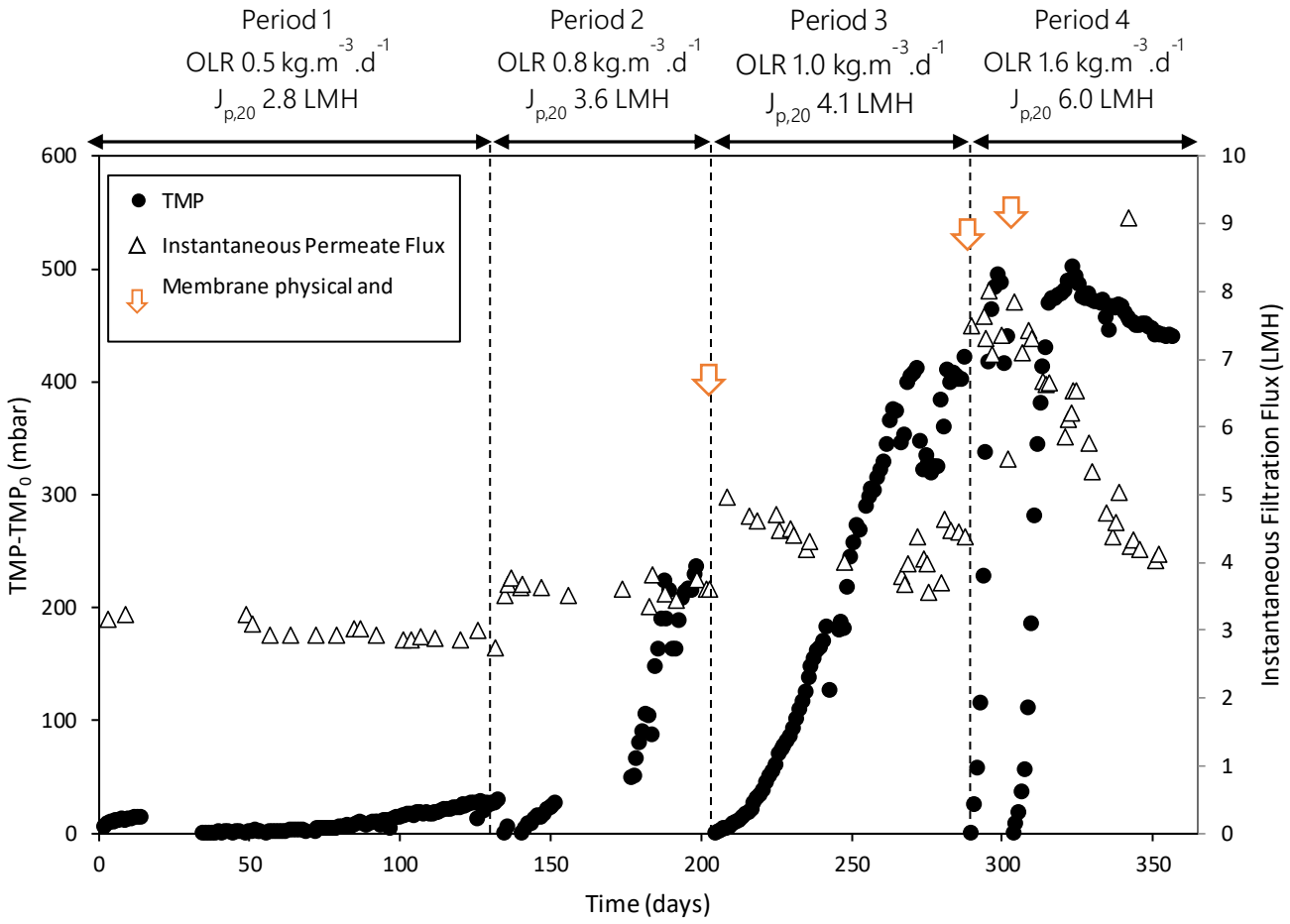

382

383 Fig. 2 – Transmembrane pressure and instantaneous filtration flux during the operational periods.

384 **3.3.2 Membrane fouling resistances**

385 The extent of reversibility of the fouling layer was evaluated based on the distribution of the
386 fouling resistances (Table 6). Because the fouling rate in Period 1 was very low (Table 5) and
387 the TMP on day 134 was approximately 50 mbar, no membrane cleaning was performed
388 between Period 1 and Period 2. Therefore, no membrane fouling resistance distribution is
389 available for Period 1. Fouling resistance (R_f) corresponded to 15.0 ± 1.1 × 10^{12}, 16.8 ± 0.6 ×
390 10^{12} and 25.7 ± 4.7 × 10^{12} m^{-1} for periods 2, 3 and 4, respectively. These results demonstrate
391 that R_f was strongly correlated to permeate flux and OLR ($r > 0.99$, $p < 0.05$). $R_{reversible}$
392 accounted for 100%, 97.9% and 97.7% of the membrane fouling resistance, indicating that
393 fouling was mostly reversible under all the operating conditions tested. External deposition,
394 especially in the cake layer, was the main mechanism involved in G-AnMBR fouling, in

agreement with previous studies (Anjum et al., 2021; Kaya et al., 2017; Lin et al., 2013). Only residual fouling of $0.1 \pm 0.0 \times 10^{12}$ and $0.2 \pm 0.1 \times 10^{12}$ m^{-1} were measured for periods 3 and 4. High filtration fluxes have been observed to promote the extent of intermediate pore blocking in the early filtration step, which may lead to more severe or resistant fouling (Lin et al., 2013; Yao et al., 2022). However, the contribution of residual fouling to the total resistance was minor in comparison to the clean membrane ($R_m = 0.8 \pm 0.1 \times 10^{12}$ m^{-1}).

These results are promising for mitigation of G-AnMBR fouling, suggesting that a well-designed backwash (i.e., physical cleaning) could lead to longer filtration performance. Further research is needed to optimize the backwash parameters, such as intensity, frequency and duration, for the purpose of developing sustainable G-AnMBR domestic wastewater treatment.

Table 6 – Fouling resistance distribution for experimental periods 2, 3 and 4.

Resistances	Units	Period 2	Period 3	Period 4
$R_{fouling}$	$\times 10^{12}$ m^{-1}	15.0 ± 1.1 (100%)	16.8 ± 0.6 (100%)	25.7 ± 4.7 (100%)
$R_{reversible}$	$\times 10^{12}$ m^{-1}	15.0 ± 1.1 (100%)	16.4 ± 0.7 (97.9%)	25.1 ± 4.6 (97.7%)
$R_{irreversible}$	$\times 10^{12}$ m^{-1}	–	0.3 ± 0.1 (1.9%)	0.4 ± 0.1 (1.6%)
$R_{residual}$	$\times 10^{12}$ m^{-1}	–	0.1 ± 0.0 (0.2%)	0.2 ± 0.1 (0.8%)

3.3.3 Membrane foulants characteristization

The composition of the reversible fouling was characterized through 3DEEM analysis (Fig. 3a), while the 3DEEM content of mixed liquor and permeate have been analyzed and published in previously published study (Sanchez et al., 2022). Based on previous works, three regions of fluorophores were distinguished, namely (a) region I + II, associated with protein-like molecules, (b) region IV, corresponding to soluble microbial product (SMP)-like molecules, and (c) region III + V, related to humic substances (Chen et al., 2003; Jacquin et al., 2017) (see Fig. A2). Since polysaccharides are not analyzed through fluorescence excitation emission,

415 additional foulant characterization were performed through PN and PS quantification (Fig. 3b).
416 Among the three fluorescent regions investigated, the major volume of fluorescence belonged
417 to region I + II (72–85%), relating to colloidal and macromolecular protein-*like* compounds
418 (Jacquin et al., 2017). In addition, between 11% and 20% of the total fluorescence volume was
419 part of region III + V, corresponding to humic substances. Measurement of PN and PS contents,
420 presented in Fig. 3b, corroborates the predominance of PN materials within the fouling layer,
421 with proportions of PN approximately 55%, 77% and 84% for periods 2, 3 and 4, respectively.
422 It can therefore be assumed that PN in the form of colloidal materials and macromolecules
423 prevailed in the G-AnMBR foulant, in accordance with previous observations (R. Chen et al.,
424 2017a; Yao et al., 2020; Zhou et al., 2016). The PN to PS ratio (PN/PS) was found to be strongly
425 correlated with the decrease in HRT (r = –0.996, $p < 0.05$), demonstrating the rise in PN
426 concentration in the cake layer during the experimental periods. Several factors, including the
427 following, may be responsible for this phenomenon: (i) the increase of the permeate flux leads
428 to higher OLRs, which promote the growth of biomass and biopolymers (mainly composed of
429 PN and PS) (Huang et al., 2011); (ii) the decrease of HRT reduces degradation of polymers and
430 macromolecules because PN-based organic matter has been found to be more slowly and
431 weakly biodegradable than that based on PS, thus leading to PN accumulation (R. Chen et al.,
432 2017a; Yang et al., 2015); and (iii) PN has been reported to have higher hydrophobic
433 characteristics than PS. Accordingly, PN has more tendency to adhere to membrane surface
434 (Kaya et al., 2019).

435 Because EPS have been identified as a key factor in membrane fouling (Anjum et al., 2021; R.
436 Chen et al., 2017a; Ding et al., 2015), the fouling layer was further fractionated into SMP, LB-
437 EPS and TB-EPS to identify the contribution of EPS fractions to total fouling. Fig. 3c shows
438 the repartition of the three EPS fractions extracted from the cake layer in periods 2, 3 and 4. Of
439 the three EPS fractions, the TB-EPS were in higher proportion within the fouling layer for all

the periods, followed by the SMP content and LB-EPS content. Nonetheless, the TB-EPS content progressively decreased from 63% to 43% as the permeate flux increased from 1.8 to 3.6 LMH, respectively. Conversely, the fraction of SMPs extracted from the fouling layer increased from 9% to 31% with the increase of permeate flux. The increase in SMPs was probably caused by the OLR increase and HRT decrease, which stimulated production of SMPs and reduced their degradation (Huang et al., 2011).

On the one hand, it might be concluded that bound-EPS (TB- and LB-EPS) represented an important fraction of the foulants deposit because bound-EPS were mostly within the fouling layer, in agreement with previous studies (R. Chen et al., 2017a; Gao et al., 2011). On the other hand, the SMP fraction increased with the increase of filtration flux and fouling resistance, which could suggest that SMPs play an important role in membrane fouling. Ding et al. (2015) studied the extent of fouling caused by the three EPS fractions extracted from the cake sludge of a mesophilic AnMBR. It was found that at the same TOC concentration, SMPs caused the highest filtration resistance (50.2%) followed by LB-EPS (19.8%) and TB-EPS (30.0%). It was suggested that the SMP fraction exhibited a lower energy barrier than the bound-EPS fractions, so that SMPs needed to overcome weaker repulsive interaction energy to adhere to the membrane surface (Ding et al., 2015). Accordingly, it is important to consider both the relative contribution and specific fouling resistance when evaluating the impact of EPS fractions (i.e., SMP, LB-EPS, TB-EPS) on membrane fouling. Although no clear conclusion can be provided regarding the major EPS contributor, the abundance of bound-EPS indicated the presence of biomass attachment on the membrane surface, while the SMP revealed an implication of dissolved compounds in global membrane fouling. Therefore, it is possible to conclude that the fouling was mainly due to the combination of organic and biological fouling.

To summarize, fouling layer analysis indicated that PN materials were the main foulant in the G-AnMBR system that was studied. PN content was highly influenced by the operating

conditions. EPS clearly played a relevant role in membrane fouling. The role of EPS fractions in membrane fouling is still not clear; however, it is hypothesized that they can (i) participate in biomass–membrane bonding (bound-EPS), (ii) form a strong interaction with the membrane surface (SMPs) and (iii) create a wide EPS network, consolidating the cake layer.

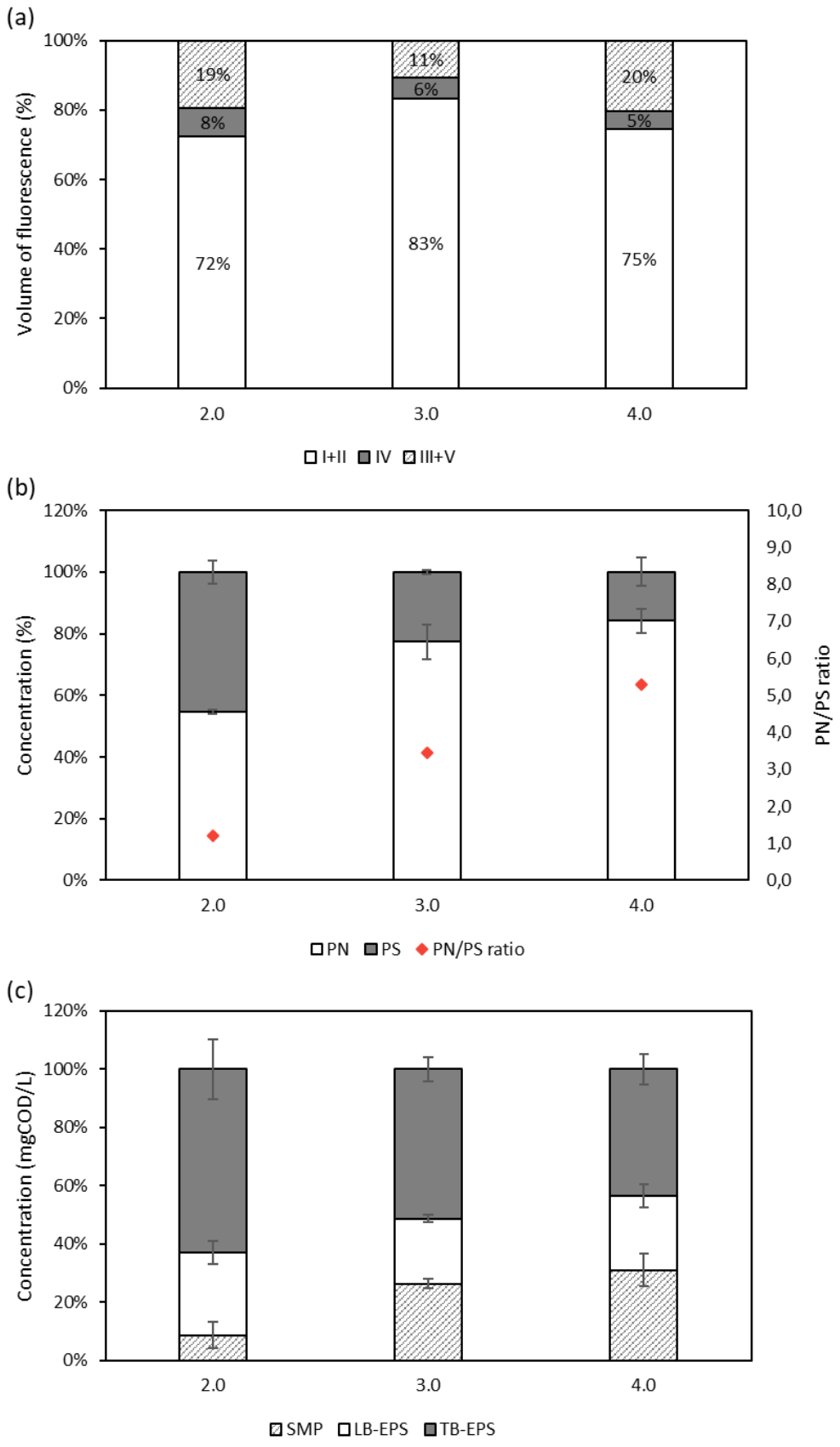

469

470 Fig. 3 – Composition of membrane foulants obtained through (a) 3DEEM (I + II: protein-*like* substances, III + V:
471 humic-*like* substances, IV: SMP-*like* molecules); (b) PN and PS concentration; (c) EPS concentration.

3.3 Preliminary economic evaluation

Fig. 4a shows the gross cost, electricity revenue and net cost for the four scenarios evaluated for a plant lifetime of 30 years. Fig. A3 and A4 of the supplementary information illustrate the same results for a plant lifetime of 20 and 40 years, respectively. The results show that scenarios 3 and 4 featured the lowest net cost for the G-AnMBR system under study. The lower net cost of these scenarios compared with scenarios 1 and 2 can be mainly attributed to the lower membrane area required. This effect indicates that operating the membrane system at $J_{20,inst}$ below 3.6 LMH is not economically competitive for a G-AnMBR system operated without gas sparging. Of note, the net cost of Scenario 3 ($Jp_{20,inst}$ 4.1 LMH) was slightly lower than Scenario 4 (6.0 LMH) (Fig. 4a). In Scenario 4, high amounts of chemicals were needed for membrane cleaning (due to the high fouling rate) with a direct impact on membrane replacement frequency. In this regard, the extra costs regarding membrane cleaning and replacement in Scenario 4 did not offset the lower membrane purchase costs when compared with Scenario 3. Accordingly, it is important to achieve a compromise solution between operating the membranes at relatively higher fluxes (CAPEX) while consuming a moderate amount of chemicals (OPEX). In this regard, further pilot- and demonstration-scale studies are necessary to determine, at larger scale, the optimum flux and chemical cleaning conditions to reduce the costs and improve the economic competitiveness of the G-AnMBR system. Besides cost considerations, the operation of the G-AnMBR operated without gas sparging has the potential to make the WWTP energy positive due to the biogas (60-70% CH_4) produced in the system (0.4-0.5 $kWh \cdot m^{-3}$).

Fig. 4b shows the gross cost distribution for the different scenarios. Detailed information regarding the distribution of the gross costs can be found in Table A4 of the supplementary information. Membrane purchase accounted for more than 49% of the gross cost for all the scenarios, although its contribution progressively decreased from 89% to 49% as the permeate

497 flux increased from 2.8 to 6.0 LMH, respectively. The chemical cleaning also featured a
498 relatively important impact on the gross cost in scenarios 2, 3 and 4. The contribution of
499 chemical cleaning sharply increased from 0.5 to 26.0% as the permeate flux increased from 2.8
500 to 6.0 LMH, respectively, because the extent of membrane fouling was substantially higher at
501 higher fluxes. This was particularly important in Scenario 4, in which the high fouling rate and
502 chemical cleaning frequency made replacement of the membrane system necessary during the
503 plant's lifetime, with a direct impact on the OPEX (see Table A4 of the supplementary
504 information). This highlights that the membrane chemical cleaning strategy is a key economic
505 driver, especially in those scenarios in which intensive chemical cleaning is needed to control
506 long-term membrane fouling. Figure 4b also shows that the bioreactor construction contribution
507 decreased from 7.1 to 3.8% as the OLR increased from 0.5 to 1.6 kgCOD m^{-3} d^{-1}, respectively.
508 This illustrates that increasing OLR has also an impact on the economic balance of the system.
509 Overall, these economic results further corroborate that achieving a trade-off between
510 increasing the flux and OLR (system intensification) without requiring intensive physical and
511 chemical cleaning strategies to control membrane fouling is important for the economics of a
512 G-AnMBR system operated in submerged mode and without gas sparging.

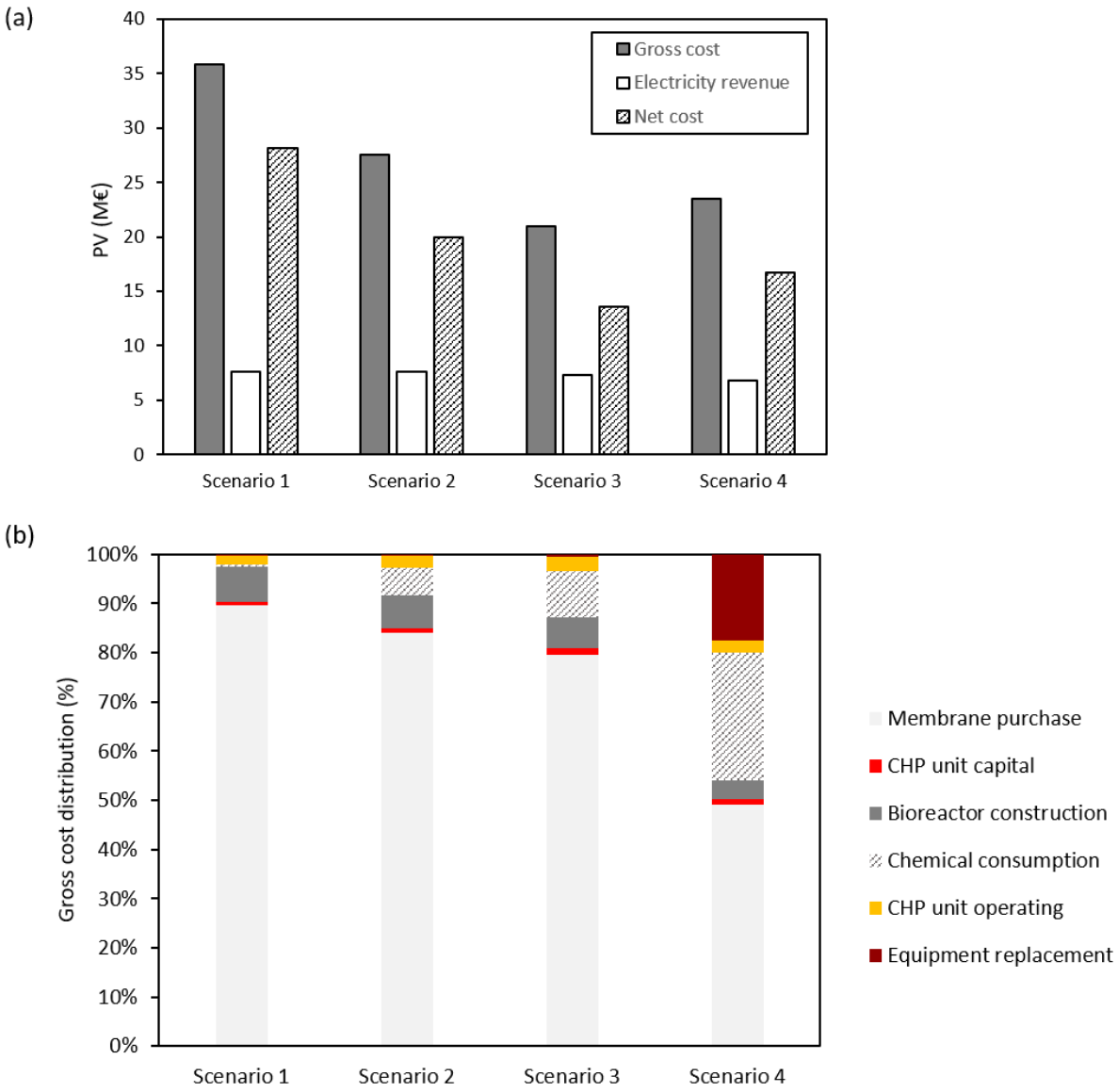

513

514 Fig. 4 – (a) Present value (PV) of the net cost, gross cost and electricity revenue; (b) gross cost distribution for
515 the four scenarios evaluated for a 30-year plant lifetime.

516

517

4. Conclusions

The present work studied the impact of design parameters (i.e., OLR, permeate flux, HRT) on a G-AnMBR operated with a submerged UF membrane and without gas sparging as fouling control for mainstream domestic wastewater at ambient temperature. Four design OLRs were tested (between 0.5 and 1.6 $kgCOD.m^{-3}.d^{-1}$) resulting in four HRT and permeate flux conditions.

- The G-AnMBR achieved a rapid steady-state and high COD removal efficiencies (>90%) for HRTs ranging between 14 and 7 h.
- The proportion of tCOD converted into methane was 77% at the lowest OLR and 70% at the highest OLR, confirming the decrease in biological activity with increasing OLR. However, more methane was recovered in the gaseous phase at the highest OLR (86% of the total methane produced) in comparison to the lowest OLR (65% of the total methane produced). Hence, at higher OLRs, the amount of bio-methane energy lost in the effluent and the greenhouse gas emissions were lowered.
- Membrane fouling increased with the permeate flux and OLR, highlighting the important role of those parameters in cake layer formation and build-up. Under all conditions, proteinaceous colloidal and macromolecules were the main components of the G-AnMBR cake layer. Membrane permeability was almost totally recovered after physical cleaning with water rinsing, demonstrating that fouling was mainly reversible.
- Finally, the economic evaluation showed that filtration flux, and the resulting membrane surface area, is a crucial parameter for G-AnMBR economics, with Scenario 3 (4.1 LMH) being the most economically favorable option.

Overall, these results have shown that achieving a compromise solution considering permeate flux, OLR and chemical cleaning for membrane fouling control is important to reduce the net cost of G-AnMBR systems operated without gas sparging.

On this basis, the G-AnMBR could be a sustainable and efficient process for domestic wastewater treatment for local applications in which important financial, technical and energy resources cannot be deployed.

Supplementary information

E-supplementary data for this work can be found in the e-version of this paper online.

Acknowledgments

This work was supported by a grant overseen by the French National Research Agency as part of the "JCJC" Program BàMAn (ANR-18-CE04-0001-01). The authors wish to acknowledge Valérie Bonniol (IEM) for her assistance in the development of the VFA quantification.

References

Anjum, F., Khan, I.M., Kim, J., Aslam, M., Blandin, G., Heran, M., Lesage, G., 2021. Trends and progress in AnMBR for domestic wastewater treatment and their impacts on process efficiency and membrane fouling. Environmental Technology & Innovation 21, 101204. https://doi.org/10.1016/j.eti.2020.101204

APHA, AWWA, WEF (Eds.), 1998. Standard methods: for the examination of water and wastewater, 20. ed. ed. American Public Health Association, Washington, DC.

Aslam, A., Khan, S.J., Shahzad, H.M.A., 2022. Anaerobic membrane bioreactors (AnMBRs) for municipal wastewater treatment- potential benefits, constraints, and future perspectives: An updated review. Science of The Total Environment 802, 149612. https://doi.org/10.1016/j.scitotenv.2021.149612

Aslam, M., Charfi, A., Lesage, G., Heran, M., Kim, J., 2017. Membrane bioreactors for wastewater treatment: A review of mechanical cleaning by scouring agents to control membrane fouling. Chemical Engineering Journal 307, 897–913. https://doi.org/10.1016/j.cej.2016.08.144

Bacchin, P., Aimar, P., Field, R.W., 2006. Critical and sustainable fluxes: Theory, experiments and applications. Journal of Membrane Science 281, 42–69. https://doi.org/10.1016/j.memsci.2006.04.014

Batstone, D.J., Virdis, B., 2014. The role of anaerobic digestion in the emerging energy economy. Current Opinion in Biotechnology, Energy biotechnology • Environmental biotechnology 27, 142–149. https://doi.org/10.1016/j.copbio.2014.01.013

Boulenger, P., Gallouin, Y., 2009. Traitements biologiques anaérobies des effluents industriels. Ed. Techniques Ingénieur.

Brepols, C., Drensla, K., Janot, A., Trimborn, M., Engelhardt, N., 2008. Strategies for chemical cleaning in large scale membrane bioreactors. Water Science and Technology 57, 457–463. https://doi.org/10.2166/wst.2008.112

Chen, C., Guo, W., Ngo, H.H., Chang, S.W., Duc Nguyen, D., Dan Nguyen, P., Bui, X.T., Wu, Y., 2017a. Impact of reactor configurations on the performance of a granular anaerobic membrane bioreactor for municipal wastewater treatment. International Biodeterioration & Biodegradation 121, 131–138. https://doi.org/10.1016/j.ibiod.2017.03.021

Chen, C., Guo, W.S., Ngo, H.H., Liu, Y., Du, B., Wei, Q., Wei, D., Nguyen, D.D., Chang, S.W., 2017b. Evaluation of a sponge assisted-granular anaerobic membrane bioreactor (SG-AnMBR) for municipal wastewater treatment. Renewable Energy 111, 620–627. https://doi.org/10.1016/j.renene.2017.04.055

Chen, R., Nie, Y., Hu, Y., Miao, R., Utashiro, T., Li, Q., Xu, M., Li, Y.-Y., 2017a. Fouling behaviour of soluble microbial products and extracellular polymeric substances in a submerged anaerobic membrane bioreactor treating low-strength wastewater at room temperature. Journal of Membrane Science 531, 1–9. https://doi.org/10.1016/j.memsci.2017.02.046

Chen, R., Nie, Y., Ji, J., Utashiro, T., Li, Q., Komori, D., Li, Y., 2017b. Submerged anaerobic membrane bioreactor (SAnMBR) performance on sewage treatment: removal efficiencies, biogas production and membrane fouling. Water science and technology 76, 1308–1317. https://doi.org/10.2166/wst.2017.240

Chen, W., Westerhoff, P., Leenheer, J.A., Booksh, K., 2003. Fluorescence Excitation−Emission Matrix Regional Integration to Quantify Spectra for Dissolved Organic Matter. Environ. Sci. Technol. 37, 5701–5710. https://doi.org/10.1021/es034354c

Chheang, M., Hongprasith, N., Ratanatawanate, C., Lohwacharin, J., 2022. Effects of Chemical Cleaning on the Ageing of Polyvinylidene Fluoride Microfiltration and Ultrafiltration

603 Membranes Fouled with Organic and Inorganic Matter. Membranes (Basel) 12, 280.
604 https://doi.org/10.3390/membranes12030280
605 Ding, Y., Tian, Y., Li, Z., Zuo, W., Zhang, J., 2015. A comprehensive study into fouling
606 properties of extracellular polymeric substance (EPS) extracted from bulk sludge and
607 cake sludge in a mesophilic anaerobic membrane bioreactor. Bioresource Technology
608 192, 105–114. https://doi.org/10.1016/j.biortech.2015.05.067
609 Dong, Q., Parker, W., Dagnew, M., 2016a. Influence of SRT and HRT on Bioprocess
610 Performance in Anaerobic Membrane Bioreactors Treating Municipal Wastewater.
611 Water Environment Research 88, 158–167.
612 https://doi.org/10.2175/106143016X14504669767175
613 Dong, Q., Parker, W., Dagnew, M., 2016b. Long term performance of membranes in an
614 anaerobic membrane bioreactor treating municipal wastewater. Chemosphere 144, 249–
615 256. https://doi.org/10.1016/j.chemosphere.2015.08.077
616 Dubois, M., Gilles, K., Hamilton, J.K., Rebers, P.A., Smith, F., 1951. A Colorimetric Method
617 for the Determination of Sugars. Nature 168, 167–167.
618 https://doi.org/10.1038/168167a0
619 Evans, P.J., Parameswaran, P., Lim, K., Bae, J., Shin, C., Ho, J., McCarty, P.L., 2019. A
620 comparative pilot-scale evaluation of gas-sparged and granular activated carbon-
621 fluidized anaerobic membrane bioreactors for domestic wastewater treatment.
622 Bioresource Technology 288, 120949. https://doi.org/10.1016/j.biortech.2019.01.072
623 Gao, W.J., Lin, H.J., Leung, K.T., Schraft, H., Liao, B.Q., 2011. Structure of cake layer in a
624 submerged anaerobic membrane bioreactor. Journal of Membrane Science 374, 110–
625 120. https://doi.org/10.1016/j.memsci.2011.03.019
626 Gouveia, J., Plaza, F., Garralon, G., Fdz-Polanco, F., Peña, M., 2015. A novel configuration for
627 an anaerobic submerged membrane bioreactor (AnSMBR). Long-term treatment of
628 municipal wastewater under psychrophilic conditions. Bioresource Technology 198,
629 510–519. https://doi.org/10.1016/j.biortech.2015.09.039
630 Hu, Y., Yang, Y., Yu, S., Wang, X.C., Tang, J., 2018. Psychrophilic anaerobic dynamic
631 membrane bioreactor for domestic wastewater treatment: Effects of organic loading and
632 sludge recycling. Bioresource Technology 270, 62–69.
633 https://doi.org/10.1016/j.biortech.2018.08.128
634 Huang, Z., Ong, S.L., Ng, H.Y., 2011. Submerged anaerobic membrane bioreactor for low-
635 strength wastewater treatment: Effect of HRT and SRT on treatment performance and
636 membrane fouling. Water Research 45, 705–713.
637 https://doi.org/10.1016/j.watres.2010.08.035
638 Jacquin, C., Lesage, G., Traber, J., Pronk, W., Heran, M., 2017. Three-dimensional excitation
639 and emission matrix fluorescence (3DEEM) for quick and pseudo-quantitative
640 determination of protein- and humic-like substances in full-scale membrane bioreactor
641 (MBR). Water Res 118, 82–92. https://doi.org/10.1016/j.watres.2017.04.009
642 Jeison, D., van Lier, J.B., 2006. Cake layer formation in anaerobic submerged membrane
643 bioreactors (AnSMBR) for wastewater treatment. Journal of Membrane Science 284,
644 227–236. https://doi.org/10.1016/j.memsci.2006.07.035
645 Ji, J., Chen, Y., Hu, Y., Ohtsu, A., Ni, J., Li, Y., Sakuma, S., Hojo, T., Chen, R., Li, Y.-Y.,
646 2021a. One-year operation of a 20-L submerged anaerobic membrane bioreactor for real
647 domestic wastewater treatment at room temperature: Pursuing the optimal HRT and
648 sustainable flux. Science of The Total Environment 775, 145799.
649 https://doi.org/10.1016/j.scitotenv.2021.145799
650 Ji, J., Du, R., Ni, J., Chen, Y., Hu, Y., Qin, Y., Hojo, T., Li, Y.-Y., 2022. Submerged anaerobic
651 membrane bioreactor applied for mainstream municipal wastewater treatment at a low

temperature: Sludge yield, energy balance and membrane filtration behaviors. Journal of Cleaner Production 355, 131831. https://doi.org/10.1016/j.jclepro.2022.131831
Ji, J., Ni, J., Ohtsu, A., Isozumi, N., Hu, Y., Du, R., Chen, Y., Qin, Y., Kubota, K., Li, Y.-Y., 2021b. Important effects of temperature on treating real municipal wastewater by a submerged anaerobic membrane bioreactor: Removal efficiency, biogas, and microbial community. Bioresour Technol 336, 125306. https://doi.org/10.1016/j.biortech.2021.125306
Kaya, Y., Bacaksiz, A.M., Bayrak, H., Gönder, Z.B., Vergili, I., Hasar, H., Yilmaz, G., 2017. Treatment of chemical synthesis-based pharmaceutical wastewater in an ozonation-anaerobic membrane bioreactor (AnMBR) system. Chemical Engineering Journal 322, 293–301. https://doi.org/10.1016/j.cej.2017.03.154
Kaya, Y., Bacaksiz, A.M., Bayrak, H., Vergili, I., Gönder, Z.B., Hasar, H., Yilmaz, G., 2019. Investigation of membrane fouling in an anaerobic membrane bioreactor (AnMBR) treating pharmaceutical wastewater. Journal of Water Process Engineering 31, 100822. https://doi.org/10.1016/j.jwpe.2019.100822
Kong, Z., Li, L., Wu, J., Wang, T., Rong, C., Luo, Z., Pan, Y., Li, D., Li, Y., Huang, Y., Li, Y.-Y., 2021a. Evaluation of bio-energy recovery from the anaerobic treatment of municipal wastewater by a pilot-scale submerged anaerobic membrane bioreactor (AnMBR) at ambient temperature. Bioresource Technology 339, 125551. https://doi.org/10.1016/j.biortech.2021.125551
Kong, Z., Wu, J., Rong, C., Wang, T., Li, L., Luo, Z., Ji, J., Hanaoka, T., Sakemi, S., Ito, M., Kobayashi, S., Kobayashi, M., Qin, Y., Li, Y.-Y., 2021b. Large pilot-scale submerged anaerobic membrane bioreactor for the treatment of municipal wastewater and biogas production at 25 °C. Bioresour Technol 319, 124123. https://doi.org/10.1016/j.biortech.2020.124123
Layer, M., Adler, A., Reynaert, E., Hernandez, A., Pagni, M., Morgenroth, E., Holliger, C., Derlon, N., 2019. Organic substrate diffusibility governs microbial community composition, nutrient removal performance and kinetics of granulation of aerobic granular sludge. Water Research X 4, 100033. https://doi.org/10.1016/j.wroa.2019.100033
Lei, Z., Yang, S., Li, Y., Wen, W., Wang, X.C., Chen, R., 2018. Application of anaerobic membrane bioreactors to municipal wastewater treatment at ambient temperature: A review of achievements, challenges, and perspectives. Bioresource Technology 267, 756–768. https://doi.org/10.1016/j.biortech.2018.07.050
Li, X.Y., Yang, S.F., 2007. Influence of loosely bound extracellular polymeric substances (EPS) on the flocculation, sedimentation and dewaterability of activated sludge. Water Research 41, 1022–1030. https://doi.org/10.1016/j.watres.2006.06.037
Lin, H., Peng, W., Zhang, M., Chen, J., Hong, H., Zhang, Y., 2013. A review on anaerobic membrane bioreactors: Applications, membrane fouling and future perspectives. Desalination 314, 169–188. https://doi.org/10.1016/j.desal.2013.01.019
Lowry, OliverH., Rosebrough, NiraJ., Farr, A.L., Randall, RoseJ., 1951. Protein measurement with the Folin phenol reagent. Journal of Biological Chemistry 193, 265–275. https://doi.org/10.1016/S0021-9258(19)52451-6
Maaz, M., Yasin, M., Aslam, M., Kumar, G., Atabani, A.E., Idrees, M., Anjum, F., Jamil, F., Ahmad, R., Khan, A.L., Lesage, G., Heran, M., Kim, J., 2019. Anaerobic membrane bioreactors for wastewater treatment: Novel configurations, fouling control and energy considerations. Bioresource Technology 283, 358–372. https://doi.org/10.1016/j.biortech.2019.03.061
Martinez-Sosa, D., Helmreich, B., Netter, T., Paris, S., Bischof, F., Horn, H., 2011. Anaerobic submerged membrane bioreactor (AnSMBR) for municipal wastewater treatment under

mesophilic and psychrophilic temperature conditions. Bioresource Technology 102, 10377–10385. https://doi.org/10.1016/j.biortech.2011.09.012

Martin-Garcia, I., Mokosch, M., Soares, A., Pidou, M., Jefferson, B., 2013. Impact on reactor configuration on the performance of anaerobic MBRs: Treatment of settled sewage in temperate climates. Water Research 47, 4853–4860. https://doi.org/10.1016/j.watres.2013.05.008

Nie, Y., Kato, H., Sugo, T., Hojo, T., Tian, X., Li, Y.-Y., 2017. Effect of anionic surfactant inhibition on sewage treatment by a submerged anaerobic membrane bioreactor: Efficiency, sludge activity and methane recovery. Chemical Engineering Journal 315, 83–91. https://doi.org/10.1016/j.cej.2017.01.022

Plevri, A., Mamais, D., Noutsopoulos, C., 2021. Anaerobic MBR technology for treating municipal wastewater at ambient temperatures. Chemosphere 275, 129961. https://doi.org/10.1016/j.chemosphere.2021.129961

Quek, P.J., Yeap, T.S., Ng, H.Y., 2017. Applicability of upflow anaerobic sludge blanket and dynamic membrane-coupled process for the treatment of municipal wastewater. Appl Microbiol Biotechnol 101, 6531–6540. https://doi.org/10.1007/s00253-017-8358-6

Robles, Á., Durán, F., Giménez, J.B., Jiménez, E., Ribes, J., Serralta, J., Seco, A., Ferrer, J., Rogalla, F., 2020. Anaerobic membrane bioreactors (AnMBR) treating urban wastewater in mild climates. Bioresource Technology 314, 123763. https://doi.org/10.1016/j.biortech.2020.123763

Robles, A., Ruano, M.V., Ribes, J., Seco, A., Ferrer, J., 2014. Model-based automatic tuning of a filtration control system for submerged anaerobic membrane bioreactors (AnMBR). Journal of Membrane Science 465, 14–26. https://doi.org/10.1016/j.memsci.2014.04.012

Rong, C., Luo, Z., Wang, T., Guo, Y., Kong, Z., Wu, J., Ji, J., Qin, Y., Hanaoka, T., Sakemi, S., Ito, M., Kobayashi, S., Kobayashi, M., Li, Y.-Y., 2021. Chemical oxygen demand and nitrogen transformation in a large pilot-scale plant with a combined submerged anaerobic membrane bioreactor and one-stage partial nitritation-anammox for treating mainstream wastewater at 25 °C. Bioresource Technology 341, 125840. https://doi.org/10.1016/j.biortech.2021.125840

Ruigómez, I., Vera, L., González, E., González, G., Rodríguez-Sevilla, J., 2016a. A novel rotating HF membrane to control fouling on anaerobic membrane bioreactors treating wastewater. Journal of Membrane Science 501, 45–52. https://doi.org/10.1016/j.memsci.2015.12.011

Ruigómez, I., Vera, L., González, E., Rodríguez-Sevilla, J., 2016b. Pilot plant study of a new rotating hollow fibre membrane module for improved performance of an anaerobic submerged MBR. Journal of Membrane Science 514, 105–113. https://doi.org/10.1016/j.memsci.2016.04.061

Sanchez, L., Carrier, M., Cartier, J., Charmette, C., Heran, M., Steyer, J.-P., Lesage, G., 2022. Enhanced organic degradation and biogas production of domestic wastewater at psychrophilic temperature through submerged granular anaerobic membrane bioreactor for energy-positive treatment. Bioresource Technology 353, 127145. https://doi.org/10.1016/j.biortech.2022.127145

Shin, C., Tilmans, S.H., Chen, F., McCarty, P.L., Criddle, C.S., 2021. Temperate climate energy-positive anaerobic secondary treatment of domestic wastewater at pilot-scale. Water Research 204, 117598. https://doi.org/10.1016/j.watres.2021.117598

Smith, A.L., Skerlos, S.J., Raskin, L., 2013. Psychrophilic anaerobic membrane bioreactor treatment of domestic wastewater. Water Research 47, 1655–1665. https://doi.org/10.1016/j.watres.2012.12.028

751 Smith, A.L., Stadler, L.B., Cao, L., Love, N.G., Raskin, L., Skerlos, S.J., 2014. Navigating
752 Wastewater Energy Recovery Strategies: A Life Cycle Comparison of Anaerobic
753 Membrane Bioreactor and Conventional Treatment Systems with Anaerobic Digestion.
754 Environ. Sci. Technol. 48, 5972–5981. https://doi.org/10.1021/es5006169
755 Smith, A.L., Stadler, L.B., Love, N.G., Skerlos, S.J., Raskin, L., 2012. Perspectives on
756 anaerobic membrane bioreactor treatment of domestic wastewater: A critical review.
757 Bioresource Technology 122, 149–159. https://doi.org/10.1016/j.biortech.2012.04.055
758 Stuckey, D.C., 2012. Recent developments in anaerobic membrane reactors. Bioresource
759 Technology, Membrane Bioreactors (MBRs): State-of-Art and Future 122, 137–148.
760 https://doi.org/10.1016/j.biortech.2012.05.138
761 van Lier, J.B., Mahmoud, N., Zeeman, G., 2008. Anaerobic Wastewater Treatment, in:
762 Biological Wastewater Treatment: Principles, Medelling and Design. IWA Publishing.
763 Vinardell, S., Astals, S., Peces, M., Cardete, M.A., Fernández, I., Mata-Alvarez, J., Dosta, J.,
764 2020. Advances in anaerobic membrane bioreactor technology for municipal
765 wastewater treatment: A 2020 updated review. Renewable and Sustainable Energy
766 Reviews 130, 109936. https://doi.org/10.1016/j.rser.2020.109936
767 Vinardell, S., Sanchez, L., Astals, S., Mata-Alvarez, J., Dosta, J., Heran, M., Lesage, G., 2022.
768 Impact of permeate flux and gas sparging rate on membrane performance and process
769 economics of granular anaerobic membrane bioreactors. Science of The Total
770 Environment 825, 153907. https://doi.org/10.1016/j.scitotenv.2022.153907
771 Wang, K.M., Cingolani, D., Eusebi, A.L., Soares, A., Jefferson, B., McAdam, E.J., 2018.
772 Identification of gas sparging regimes for granular anaerobic membrane bioreactor to
773 enable energy neutral municipal wastewater treatment. Journal of Membrane Science
774 555, 125–133. https://doi.org/10.1016/j.memsci.2018.03.032
775 Watanabe, R., Nie, Y., Wakahara, S., Komori, D., Li, Y.-Y., 2017. Investigation on the response
776 of anaerobic membrane bioreactor to temperature decrease from 25°C to 10°C in
777 sewage treatment. Bioresource Technology 243, 747–754.
778 https://doi.org/10.1016/j.biortech.2017.07.001
779 Yang, G., Zhang, P., Zhang, G., Wang, Y., Yang, A., 2015. Degradation properties of protein
780 and carbohydrate during sludge anaerobic digestion. Bioresource Technology 192, 126–
781 130. https://doi.org/10.1016/j.biortech.2015.05.076
782 Yang, Y., Zang, Y., Hu, Y., Wang, X.C., Ngo, H.H., 2020. Upflow anaerobic dynamic
783 membrane bioreactor (AnDMBR) for wastewater treatment at room temperature and
784 short HRTs: Process characteristics and practical applicability. Chemical Engineering
785 Journal 383, 123186. https://doi.org/10.1016/j.cej.2019.123186
786 Yao, W., Hou, L., Wang, F., Wang, Z., Zhang, H., 2022. Dual-objective for the mechanism of
787 membrane fouling in the early stage of filtration and determination of cleaning
788 frequency: A novel combined model. Journal of Membrane Science 647, 120315.
789 https://doi.org/10.1016/j.memsci.2022.120315
790 Yao, Y., Zhou, Z., Stuckey, D.C., Meng, F., 2020. Micro-particles—A Neglected but Critical
791 Cause of Different Membrane Fouling between Aerobic and Anaerobic Membrane
792 Bioreactors. ACS Sustainable Chem. Eng. 8, 16680–16690.
793 https://doi.org/10.1021/acssuschemeng.0c06502
794 Yeo, H., An, J., Reid, R., Rittmann, B.E., Lee, H.-S., 2015. Contribution of Liquid/Gas Mass-
795 Transfer Limitations to Dissolved Methane Oversaturation in Anaerobic Treatment of
796 Dilute Wastewater. Environ. Sci. Technol. 49, 10366–10372.
797 https://doi.org/10.1021/acs.est.5b02560
798 Zhou, Z., Tan, Y., Xiao, Y., Stuckey, D.C., 2016. Characterization and Significance of Sub-
799 Visible Particles and Colloids in a Submerged Anaerobic Membrane Bioreactor

(SAnMBR). Environ. Sci. Technol. 50, 12750–12758. https://doi.org/10.1021/acs.est.6b03581